

---

## TEM 3D-Tomography of High-Pressure Frozen Cells Reveals Detailed Viral Components in the Maturation of Semliki Forest Virus

Simon W. Ma

### Abstract

*Electron tomography (ET), using back projections for three dimensional (3D) reconstruction, complemented with the modern techniques of high-pressure freezing (HPF) and free-substitution (FS) in specimen preparation, can preserve the membrane-bound organelles of a virus-infected cell. The quality of the specimen preparation in situ limits the fidelity of structure-based observation in cellular processes during the assembly of Semliki Forest Virus (SFV) studied as a model system. For HPE, the cell specimens were treated with a fixative of osmium tetroxide (OsO<sub>4</sub>) for morphological study. After the sample was frozen, FS was used to substitute the water in the frozen specimen for subsequent Eponate-Araldite resin embedding. Three-dimensional tomograms of specimens stained with osmium provided basis morphology of viral particles because OsO<sub>4</sub> would bind at double bonds of unsaturated lipid. Using ET for reconstruction together with HPF and FS for sample preparation yielded measurements of whole viral particles that showed a consistent ratio in virus dimension, with a systematic reduction of 20% in diameter, compared with the dimensions of the isolated single particle reconstructions measured by cryo electron microscopy.*

### Introduction

Viruses cause a great deal of human misery. They are responsible for the common cold, small pox, AIDS, rashes, arthritis, and a host of other ailments and diseases. In order to study the mechanism for viral particles infecting the host cells, biological researchers seek for the viral structure, which can be revealed from well-preserved cell specimens, at the highest achievable resolution. A well studied example is Semliki forest virus (SFV), an Alphavirus. SFV was first isolated in 1944 from mosquitoes in the Semliki Forest, Uganda, by the Uganda Virus Research Institute (Kujala et al., 2001). Alphaviruses are small,

about 70 nm in diameter. Like most Alphaviruses, SFV consists of a positive single stranded RNA genome surrounded by a capsid, which is composed of protein encoded by a viral genome. With T=4 icosahedral (20 faces) symmetry, SFV has 240 proteins to form the capsid (Cheng et al., 1995). Alphaviruses enter the host cells by class II membrane fusion and mature by budding at the cell membrane. In this study, Baby Hamster Kidney (BHK) cells were infected with SFV. We studied the life cycle of this virus in order to capture the budding viral particles and to measure the whole diameter of the SFVs.

In the beginning of an EM study, the method of specimen preparation determines the quality of the final images in the tomograms. Conventional methods used to prepare cells for EM observation, including chemical fixation using both immersion and perfusion fixation, dehydration and embedding, can result in unwanted artifacts. In one study, micrograms on rat tissue showed that immersion fixation caused the smooth endoplasmic reticulum to lose its anastomosing tubular appearance and to become vesicular (Bozzola et al., 1992). These results caused fixation artifacts to become a subject of concern to researchers. Another concern is that the penetration of osmium, a major ingredient of fixative, is very slow (less than 0.5 mm per hour), which can result in the diffusion of the chemical reagent (Bozzola et al., 1992). Fortunately, the combination of high-pressure freezing and freeze-substitution, techniques that are commonly used in morphological studies at a higher level, can avoid these problems (Howe et al., 2001; Kirkham et al., 2003). Recently, we successfully demonstrated in two dimensional projections using electron microscopy that the ultrastructures of high-pressure frozen, thin-layer embedded yeast cells were well preserved and saved from ice crystal damage.

Subsequent to specimen preparation, the BHK cells infected with SFVs were embedded in a thin layer of polymerized resin. Using this method, an individual virus in the native environment can be viewed by high-resolution electron microscopy to pre-select the budding stages of that virus before running electron microscopic tomography (ET). By using back projections, ET can produce 3D images of viruses that show viral assemblies such as the nucleocapsid, lipid bilayer and envelope proteins in their physiologically functioning stages. The resolution of such tomograms commonly ranges from 3 nm to 8 nm (Marko et al., 2000; Cheng et al., 2001; Wartiovaara et al., 2004).

## Materials and Methods

### HIGH PRESSURE FREEZING

Having the gold plated flat specimen carriers (Figure 1e) lodged in the loaded carrier (1d), we used a fine-tipped paint brush to immediately transfer the cell specimens that had just been filtered to the 2mm wide and 100  $\mu$ m deep specimen carriers. This step was performed under a stereoscope. After the specimen carriers were screwed into the flat specimen pod (1b), we connected the pod to the loading device (1a). Finally, the latter loading device was inserted into the high-pressure freezing machine (Leica EMPact). One major advantage of using HPF is that the specimens are frozen at a very high pressure (1,200 bars). HPF works effectively as a physical cryoprotectant to reduce ice crystal formation and damage; using alternative cryoprotectant measures such as the application of sucrose, glucose, or glycerol may obscure some surface features because they are not sublimed away easily (Revel et al., 1983; Watson et al., 1984).

### FREEZE-SUBSTITUTION AND INFILTRATION WITH RESIN

For freeze-substitution, specimens were quickly transferred to pre-cooled cryovials (-80°C) containing the fixative solution. For conventional studies, the specimens were soaked in anhydrous acetone containing 1% OsO<sub>4</sub>, Osmium tetroxide and 0.1% UA, Uranyl acetate (McDonald & Muller Reichert, 2002; Wartiovaara et al., 2004). The latter fixative solution was then stored in the freeze-

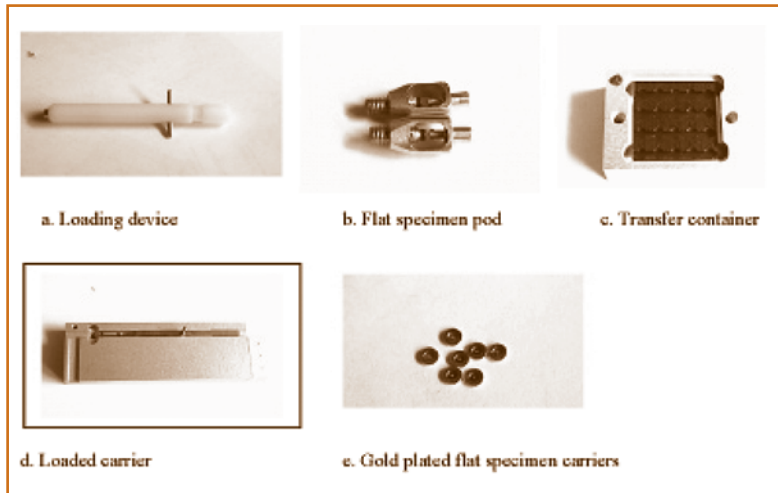


**Figure 1.** HPF apparatus. The Leica EMPact comes with many delicate accessories. The naming of the equipment can be confusing because the names have not been used consistently throughout the literature. For simplicity, the names used in this paper refer to the physical objects displayed here.

substitution machine (Leica AFS) for about 4 days (see Figure 2).

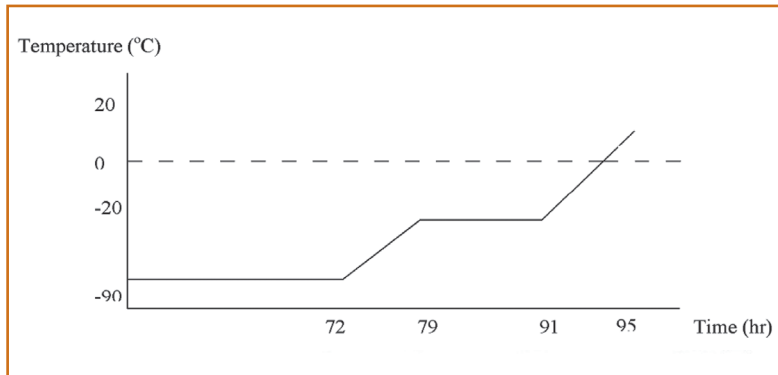


**Figure 2.** Schedule for FS. Liquid N<sub>2</sub> was used to maintain the starting temperature at -90°C for 72 hours. The time was increased to 79 hours with a temperature increment of 10°C per hour. The fixative solution with cell specimens was then kept at 79°C for 12 hours, followed by an increase to 20 °C at a rate of 10 °C per hour.

After 95 hours of free-substitution, the fixative solution was carefully rinsed out with three consecutive 5-minute changes of pure acetone in order to wash away any unreacted reagents. After removing the samples from the gold plated flat specimen carriers, the samples were then infiltrated with appropriate ratios of pure acetone to pure resin mixtures and pure resin according to the schedule seen in Table 1.

The Eponate-12 Araldite resin was made according to the published procedures. Fresh “degassed” resin with accelerator was used to replace the original resin before being placed in a 65° C oven for a minimum of 48 hours for well polymerization.

Mixture	Time
<i>Acetone resin (3-1)</i>	1 hr.
<i>Acetone resin (2-2)</i>	1 hr.
<i>Acetone resin (1-3)</i>	2 hrs.
<i>Pure resin</i>	1 hr.
<i>Pure resin</i>	overnight
<i>Pure resin</i>	1 hr.

**Table 1.** Scheme for resin infiltration. The left column gives the mixture of embedding materials for morphological study, and the right column lists the corresponding time. The general principle of infiltration is gradually to replace water within the cell (by washing with acetone) with embedding media. Eponate-12 araldite is introduced gradually into the cell specimens until the pure resin is used. A minimum of 18 hrs. is required. A longer time for infiltration is encouraged for optimum results.

## SECTIONING AND POST-STAINING

After polymerization, the cell specimens were mounted on the tip of the hard resin block for ultramicrotomy. Longitudinal sections were cut through the block using the Leica Ultracut UCT Microtome. Thin section cutting is a very time-consuming and painstaking process; a step-wise process of thin section cutting was carried out using standard techniques for electron microscopy (Sorvall 1967). Both thin (80nm) and semi-thick (150nm) Eponate-12 Araldite sections were collected on formvar-coated copper slot grids and contrasted with 4% UA in 70% ethanol followed by lead citrate.

## TOMOGRAPHIC RECONSTRUCTION OF VIRAL PARTICLES

A JOEL JEM-4000 FX, operating at 400 KV, was used for viewing the 150nm sections, and a Zeiss (LEO) 910, operating at 120KV, was used for most of the 80nm sections. In both cases, 10nm colloidal gold particles were placed on both faces of a slot grid in order to work as fiduciary markers for the following image processing, and the sections were positioned in a rotation holder. Some of the sections were mounted in a liquid nitrogen cryo-specimen holder, and prior to tilting were then pre-irradiated with at least 10,000  $\text{e}^-/\text{nm}^2$  in order to minimize the mass lost due to electron exposure (Luther, 1992). Micrograms were taken from  $+60^\circ$  to  $-60^\circ$  with a gradual increment of  $1^\circ$  or  $2^\circ$  along the electron beam, or the Z-axis. In order to obtain the best reconstruction quality, both single- and dual-axis tilt series tomograms were constructed from a range of 120 degrees of tilt (Wartiovaara et al., 2004).

The recording and reconstruction pixel size was 1.0 nm and 0.5 nm, the smaller being used for the thinner sections. The electron dose for each image was 500-1000  $\text{e}^-/\text{nm}^2$ . The micrographs were digitized with 1 K slow-CCD camera, and the tomographic reconstruction program, SPIDER, used the gold particles to align the serial projections (Penczek et al., 1998; Cheng et al., 2001) and to collect 3D volumes.

## MEASUREMENT OF VIRAL COMPONENTS

Since SFV has T=4 icosahedral symmetry, the overall shape of SFV is spherical. As shown in the SFV model (Figure 3B), the smallest circle "A" (light gray) represents the nucleocapsid, the outer ring "B" (dark gray) represents the lipid bilayer, and the outermost ring "C" (black) represents the envelope protein of the SFV. For simplicity, a diameter was drawn (see Figure 3A); hence, the dimensions of the three abovementioned major viral components were measured by analogy by finding the distance between a set of coordinates in space.

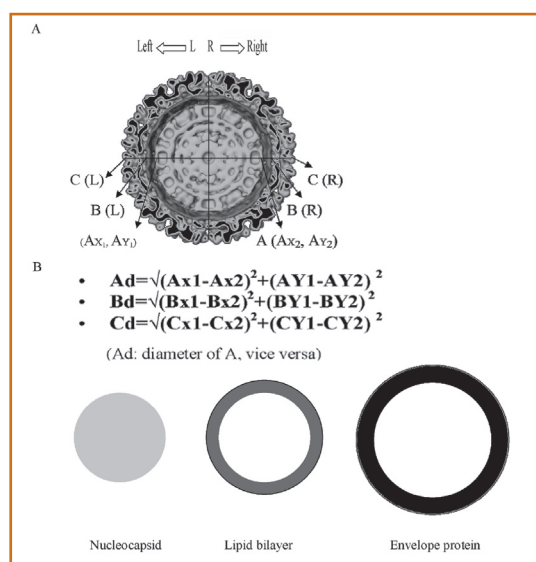


**Figure 3.** Dimensions of A (nucleocapsid), B (lipid bilayer), and C (envelope protein). A, From the simple model for the measurement of reconstructed SFV in XY plane shown in Figure 4A, the inner circle A (light gray) represents the 2D cross section of the particle's nucleocapsid. Two straight lines (perpendicular to each other) were drawn through the center of A. The X, Y coordinates were then collected by tracing along the perimeter. The same analogy was applied to B and C. In B, the equation for finding the distance between 2 points was manipulated to calculate the dimensions of the three major viral components.

The major viral components, such as the nucleocapsid, the lipid bilayer, and the spike proteins of the SFV, can be inspected by an image processing program called Robem, which can shuffle through each of the three axes (X, Y, or Z). Manual contouring on many tomographic slices is required for the measurement. First, viral particles were boxed before they were used for the measurement; the cross sections were then used as a platform for finding the matured viral particles that have the biggest size. The center of a mature viral particle could be determined after we had identified the largest cross section in the XY plane. Next, the perimeter of a particle was traced and fitted into an eclipse of the area equal to that of the traced polygon (Bashein and Detemer, 1994). Finally, another image processing program called 3dmod was used to measure the coordinates. Figure 4A shows that three screens can be opened simultaneously, which is helpful when the coordinates in the three orthogonal planes are traced manually. For example, one screen focused on the XY plane in which the particle size was measured and utilized the appearance of the XZ and YZ planes on the same window to help reach a point of agreement on an optimum set of coordinates. The same steps can be repeated for the other two planes. Images that were taken along the  $\epsilon$  beam (Z-axis) gave the most information and the best obtainable quality of the tomograms among the three axes (Zheng 2004).

**Results**

Based on six different scenarios of budding viral particles reconstructed by electron tomography, we measured the mean dimensions of matured SFV as well as the ratios of the major viral components around the mean in X, Y and Z axes. These measurements are important for interpreting the scheme of the envelope assembly and the budding process.

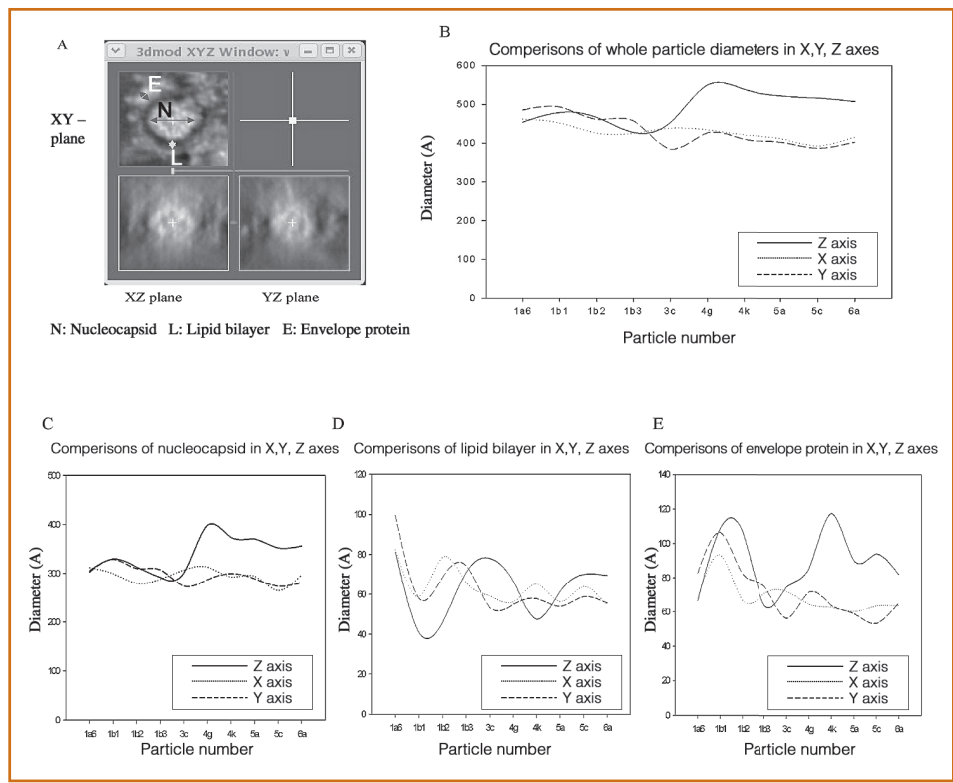


**Figure 4.** Size variations of budding viral particles. A, a cross-section of SFV in 3D volume, shows the basic viral morphology after reconstruction. Size variation of major viral components such as the nucleocapsid, lipid bilayer and envelope proteins were calculated and compared in C-E. B, group two particles (4g-6a), are obviously larger than group one particles (1a6-3c) in the Z direction. C, D, and E have the same trend of size distribution to that in B.

The size distribution of the nucleocapsid of ten budding SFVs is shown in Figure 4C. The X-axis shows particle identity (or number), and the Y-axis shows dimensions in angstroms. As illustrated in Figure 4C, nucleocapsid sizes were almost the same in both YZ and XZ planes, and the sizes were consistent in all particles. However, the nucleocapsid sizes were bigger in the XY plane, and seemed to fall into two major distributions. Particles from 1a6 to 3c were closely associated and smaller than other closely associated particle groups from 4g to 6a. For convenience, we categorized particles 1a6 to 3c as group one particles, and particles 4g to 6a as group two particles. The comparisons of lipid bilayer and of envelope protein along the three axes shown in Figure 4D and 4E revealed the same trend.

Average diameter of whole particle from 1a6-3C (group one)	Z-axis: 461 Å			
	Y-axis: 457 Å			
	X-axis: 435 Å			
Largest percent difference	=5.6%			
A				
Average diameter of whole particle from 4g to 6a (group two)	z-axis: 526 Å			
	Y-axis: 423 Å			
	X-axis: 425 Å			
Percent difference of X/Y axis	0.47 %			
Percent difference of Z to X/Y axes	19.6%			
B				
Ratios of major components to the avg. diameter of whole viral particles (4g-6a)	Avg. diameter of whole particles (in Å)	Avg. nucleocapsid (in Å)	Avg. lipid bilayer (in Å)	Avg. envelope protein (in Å)
Z-axis	526	368 (69.96%)	63 (11.98%)	98 (18.63%)
Y-axis	423	283 (66.9%)	46 (10.87%)	58 (13.7%)
X-axis	425	278 (65.4%)	48 (18.35%)	59 (13.87%)
C				

**Table 2.** Dimensions of major viral components, and their percentage of the overall particle size. In A, we see that the average diameter of group one particles is very close to each other. The percent difference in the size of the Z-axis (biggest) and the X-axis (smallest) is only 5.6%, so the particle size distribution can be considered relatively equal. In B, there is a 19.6% difference, which clearly shows that the particle size distribution between the Z and X/Y axes varied. In C, even though the major viral components vary in size in the three orthogonal planes, the ratios of the major viral components to the overall particle size turned out to be similar.

The statistical analysis in Table 2 summarizes the size distribution of the whole particle diameter. The average whole particle diameters of group one particles were calculated: an average of 461 Å along the Z-axis, 457 Å along the Y-axis, and 435 Å along the X-axis. The biggest percent difference among the three axes is 5.6%, which means these particles were almost identical in size. Furthermore, the average whole particle diameters of group 2 particles were 526 Å, 423 Å and 425 Å when measured along the Z, Y and X axes, respectively. Unlike the small percent difference (5.6%) between Z- and Y-axes for particles

from 1a6 to 3c, the percent difference between Z-axis and X/Y axis is 19.6% for particles from 4g to 6a, which justifies the categorizing of the particles into two groups. Since the goal of this experiment was to determine the size of matured SFV, group two particles with larger diameter were considered for further data analysis. Part C of Table 2 shows the ratios of the nucleocapsid, lipid bilayer and envelope protein to the whole particles' diameter measured in XY, YZ and XZ planes. Interestingly, these ratios are very close to each other in the three different orthogonal planes even though the measured diameters of whole particles along the Z-axis were 19.6% greater on average than those along the X/Y axes.

## Discussion

Electron tomography is a suitable method for reconstructing the budding viral particles in BHK cells because it allows for the identification of membrane-bounded structures, the counting of the membrane-bound particles, the determination of the variance in particles size, and the capture of the mature viral particles.

After studying a number of budding viral particles of various sizes, it appeared that the dimensions of viral particles from reconstruction varied in the three orthogonal planes even when we measured the same particles from the same 3D reconstructed volume. Using the mean particle diameter (526 Å) in this study and assuming that particle 4g is matured, we found that there is a 20% size shrinkage when compared with measurements taken using single particle reconstruction (680 Å). Distortion within a single section has been the subject of speculation for many years (Bennett, 1974; Cheng and Deatherage; Luther et al., 1988). Our research corroborates the finding that the measurement in the Z-axis provides the greatest number of image characteristics and hence the best image resolution among the three axes.

In the reconstruction made from tilted sections of Eponate-12 araldite resin embedded with viral particles, it was consistently found that there was a variation in size distribution of group two particles in the Z direction, whereas the measurements made on the same group of particles did not show such size variation in the X or Y axes. Although the reconstruction was made from a limited tilt series, it has been demonstrated (McIntosh, et al., 2005) that in an Eponate section under EM operating conditions, the tilted series, restricted from +60° to -60° in this case, should not affect image characteristics.

Whether the distortion is caused by a vacuum, electron exposure (McIntosh, et al., 2005) or both, this almost linear shrinkage in the size of viral particles suggests that the collected data in X and Y axes are consistently about 20% smaller than those of the Z-axis. The chemistry of embedding is altered by the electron beam, leading to some loss of mass from the section and an associated collapse of section thickness. Some papers have reported that the shrinkage in XY plane is modest (5-10%), whereas the shrinkage in YZ or XZ plane is severe (20-50%) (Luther, 1988; Luther, 1992). In principle, the shrinkage in the middle part of the section along the tilt axis should be minimal. Our results show that the budding-out viral particles have a linear collapse, a finding that is consistent with the published literature (Bennett, 1974; Luther et. al., 1988). However, one should realize that both Luther (1988) and Bennett (1974) have proposed that section shrinkage can occur with no cellular molecule enclosure. In the future, we hope to go beyond the morphological study of SFVs to a more important biochemical approach. An immunocytochemical experiment is under way in an effort to understand the localization and processing involved in SFV assembly.

## Acknowledgments

The author is grateful to Dr. Holland Cheng, Ph.D., for helpful comments on the manuscript, and to our colleagues Joe Wang and Pan Soonsawad for many valuable discussions. This work was supported by funds from H. Cheng Advance Microscopy & Proteomics (amp).

## References

1. Kujala, P., A. Ikaheimonen, et al. (2001). Biogenesis of the Semliki Forest Virus RNA replication complex. *J. Virology*, 75, 3873-3884.
2. Cheng R. H., J. Kuhn, N. H. Olson, M. G. Rossmann, H. K. Choi, T. J. Smith, and T. S. Baker (1995). Nucleocapsid and glycoprotein organization of an enveloped virus. *Cell*, 80, 621-630.
3. Bozzola, J. J., and L. D. Russell. *Electron Microscopy*. Boston: Jones and Bartlett, 1992.
4. Marko, M., E. C. Hsieh, et al. (2000). "Electron tomography of frozen-hydrated samples." *MSA* 310-311.
5. Cheng, R.H., K. Hultenby, L. Haag, K. Forsell, H. Garoff, C. Hsieh, and M. Marko (2001). Bring together high-and low-resolution data: Electron tomography of budding enveloped alphavirus. *Microsc Microanal*, 7S, 104-105.
6. Wartiovaara, J., L. G. Ofverstedt, J. Khoshnoodi, J. Zhang, E. Makela, S. Sandin, V. Ruotsalainen, R. H. Cheng, H. Jalanko, U. Skogglund, and K. Tryggvason (2004). Nephrin strands contribute to a porous scaffold in the renal glomerular slit diaphragm. *J Clin Invest*, 114, 1475-83.
7. Howe, M., K. McDonald, D. G. Albertson, & B. J. Meyer (2001). HIM-10 is require for kinetochore structure and function on *Caenorhabditis elegans* holocentric chromosomes, *J. Cell Biol.*, 153, 1227-1238.
8. Kirkham, M., T. Muller-Reichert, K. Oegema, S. Grill, & A. A. Hyman (2003). SAS-4 is a *C. elegans* centriolar protein that controls centrosome size. *Cell*, 112, 575-587.
9. Bennett, P.M. (1974). Decrease in section thickness on exposure to the electron beam; the use of tilted sections in estimating the amount of shrinkage. *J. Cell Sci.*, 15: 693-701.
10. Cheng, N., and J. F. Deatherage (1989). Three-dimensional reconstruction of the Z disk of sectioned bee flight muscle. *J. Cell Biol.*, 108: 1761-1774.
11. Luther, P.K. (1992). Sample shrinkage and radiation damage. In: *Electron Tomography: Three-Dimensional Imaging with the Transmission Electron Microscope*. J. Frank, ed. Plenum Press, New York, pp. 39-60.
12. Luther, P. K., M. C. Lawrence, and R. A. Crowther (1988). A method for monitoring the collapse of plastic sections as a function of electron dose. *Ultramicroscopy*, 24: 7-18.
13. Revel, J. P., T. Barnar, G. H. Haggis, and S. A. Bhatt, eds. 1983. *The science of biological specimen preparation for microscopy and microanalysis*. Scanning Electron Microscopy, Inc. (AMF O' Hare, IL). 245 pp.
14. Watson, L. P., A. E. Mckee, and B. R. Merrell. 1984. Preparation of microbiological specimens for scanning electron microscopy. *Scanning Electron Microscopy II*: 45-46.
15. Mcdonald, K., & T. Muller-Reichert (2002). Cryomethods for thin section electron microscopy. *Meth. Enzymol.* 351, 96-123.
16. Sorvall, I.. *Thin Sectioning and Associated technics for Electron Mircroscopy*. Ivan Sorvall Inc: Connecticut, 1967.
17. Penczek P., R. A. Grassuci, and J. Frank (1998). The ribosome at improved resolution: new techniques for merging and orientation refinement in 3D cryo-electron microscopy of biological particles. *Ultramicroscopy* 53:251.
18. Bashein G., P. R. Detmer (1994). Centroid of a polygon. In: *Graphics gems IV* (Heckbert PS, ed), pp 3-6. New York: Academic.

19. Zheng, Q. S., M. B. Braunfeld, et al (2004). An improved strategy for automated electron microscopic tomography. *J. Structural Biology*, 147, 91-101.
20. McIntosh, R. D. Nicastro, et al (2005). New views of cells in 3D: an introduction to electron tomography. *Cell Biology*, 15, 43-51.